Chapter

The Development and Application of a Small-Scale Organic Rankine Cycle for Waste Heat Recovery

Tzu-Chen Hung and Yong-qiang Feng

Abstract

Power conversion systems based on organic Rankine cycles have been identified as a potential technology especially in converting low-grade waste heat into electricity as well as in small-scale biomass, solar, or geothermal power plants. The theoretical analysis can guide the ORC design, but cannot predict accurately the system performance. Actually, the operation characteristics of every component have a vital effect on the system performance. This chapter presents the detailed operation characteristic of a small-scale ORC. The effects of the operation parameters, the mixture working fluid and the operation strategy on system overall performance are addressed. It can be concluded that improving the system overall performance should give priority to increase the pressure drop. Whether the mixtures exhibit better thermodynamic performance than the pure working fluids depend on the operation parameters and mass fraction of mixtures. The mixture working fluids obtain a higher expander shaft power but a relatively higher BWR. The expander rotating speed for standalone operation strategy keeps rising from 2320 to 2983 rpm, whereas that of grid connect operation strategy keeps constant of 3600 rpm.

Keywords: organic Rankine cycle (ORC), operation characteristic, mixture working fluids, system generating efficiency

1. Introduction

Energy is an indispensable resource for human progress and social development, improving energy efficiency has become a global research hot spot. Meanwhile, waste heat resource utilization problem has received widespread attention. If those waste heats can be effectively utilized, it will not only provide important technical support for energy conservation, emission reduction and environmental protection, but also generate certain economic benefits. Organic Rankine cycle (ORC) was adapted as a new technology to utilize waste heat [1–3]. The principle of ORC is similar to that of Rankine cycle. The main difference is that the low-boiling organic fluid can be used to replace the water of the Rankine cycle, which can significantly reduce the final discharge temperature, thus achieving the purpose of waste heat recovery [4–8].

Recently, many scholars have conducted in-depth research on ORC system concerning on the working fluids selection, ORC performance optimization and component development. However, the theoretical analysis can guide the ORC design, but cannot predict accurately the system performance. Therefore, some researchers devoted main effort on ORC experimental studies.

Mathias et al. [9] compared the operation characteristics using piston pump and gear pump, expressing that the piston pump outperformed than the gear pump. Carraro et al. [10] integrated a multi-diaphragm positive displacement pump into a 4 kW ORC experimental prototype, and found that the pump global efficiency was about 45–48%. Xu et al. [11] used R123 to study the matching degree of the piston pump and the expander. They stated that the low pump frequency was applicable to all expander torques, while the high pump frequency was only applicable to low torques. Zhao et al. [12] studied the diaphragm pump performance under various conditions using four different working fluids. The experimental results showed that a higher volume flow rate and pressure difference led to a higher pump isentropic efficiency. Lei et al. [13] tested a roto-jet pump at different rotating speeds using R123. They illustrated that the pump efficiency was in range of 11–23%, and an increase in pump rotating speed or a decrease in mass flow rate can cause the decrease in pump efficiency. Zeleny et al. [14] proposed a modified gear pump used in micro ORC and discussed the contribution to pump different losses. They stated that as the pressure increases, the effect of mechanical losses decreased, while the volume loss was reversed. Bianchi et al. [15] applied a sliding vane pump on the ORC using R236fa. When the mass flow rate increased from 52 to 119 g/s, the pump's mechanical power increased by 289 W. Wu et al. [16] used multistage gas-liquid booster pump to improve the performance of ORC system, revealing that the maximum conversion efficiency from high-pressure air to water was 0.72. Yang et al. [17] compared experimental characteristics of three pumps, demonstrating that the maximum actual pump efficiency of multistage centrifugal pump was 58.76%. Landelle et al. [18] discussed the operation characteristic of the reciprocating pump, reporting that the reciprocating pump had eminent volumetric efficiency and the ORC efficiency decreased as cavitation margin increased. Meng et al. [19] analyzed the multistage centrifugal pump on the ORC, expressing that the maximum overall pump efficiency was 65.7%. Bianchi et al. [20] changed the heat source temperature and feed pump speed to explore the performance of micro ORC. They found that the achieved pump efficiency was ranging from 10 to 20% and the net efficiency of the system was 2.2%. Yang et al. [21] studied the key parameters of the hydraulic diaphragm metering pump. The tested efficiency and BWR were 88.7% and 0.93, respectively. Bianchi et al. [22] used the CFD model to design and analyze a sliding vane pump. The pump performance was found to be optimal at 1250 rpm and 9.7 bar. Sun et al. [23] compared three different pumps from the viewpoint of the actual cycle and the ideal cycle. The experimental results showed that the combination of a centrifugal pump and a scroll expander can maximize the isentropic efficiency of the expander. Xi et al. [24] analyzed the influence of the plunger stroke of the working fluid pump on the system performance by orthogonal analysis. The results showed that the plunger stroke had a great influence on pump power consumption and working fluid flow. Aleksandra Borsukiewicz-Gozdur [25] found that a higher pumping power required a higher cycle pressure.

Compared with the pure working fluids, the main advantage of mixtures as ORC working fluids stems from their non-isothermal phase transitions during vaporization and condensation, and hence effectively match the temperature change of heat source and cooling water. Therefore, great attention has been drawn to the mixture working fluids. Dong et al. [26] compared the thermal efficiency of high-temperature ORC system between mixture and pure working fluids, and found that the range of options for working fluids was widened by the mixture working fluids. Garg et al. [27] investigated the thermodynamic analysis using isopentane, R245fa and their mixtures, reporting that 0.7isopentane/0.3R245fa was the preferred candidate working fluid. Lecompte et al. [28] discussed the exergy efficiency of ORC

system using mixture working fluids, stating that the mixture presented 7.1–14.2% higher second law efficiency than the pure working fluids. Zhao et al. [29] analyzed the effect of composition shift of mixture working fluids on system performance, demonstrating that the composition shift significantly influenced the performance of ORC system. Liu et al. [30] investigated the effect of condensation temperature glide using mixture on ORC performance, reporting that when the increase of cooling water temperature is greater than the condensation temperature glide, an optimal working fluid mole fraction can be obtained to maximum thermodynamic performance. Furthermore, great attention has been drawn to the experimental comparison between mixture and pure working fluids. Pu et al. [31] compared the system performance using R245fa and HFE7100, showing that R245fa obtained the maximum net power output of 1.98 kW, which is 0.95 kW higher than that of HEF7100. Molés et al. [32] proposed using HCFO-1233zd-E to replace HFC-245fa, and found that the net electrical efficiency was in rage of 5–9.7%. Jung et al. [33] studied the dynamic behavior of a kW ORC test rig using R245fa/365mfc. Li et al. [34] compared the system behaviors using R245fa and R245fa/R601a.

In this chapter, the effect of mass flow rate, pressure drop, degree of superheating and condenser temperature on thermal efficiency and system generating efficiency are examined [35–36]. Several experimental investigations using pure working fluids (R123 and R245fa) of small-scale ORC test rig have been performed. However, few of them tried to fulfill the experimental comparison between pure and mixture working fluids. And therefore, two pure working fluids (R245fa, R123) and two mixtures working fluids (0.67R245fa/0.33R123 and 0.33R245fa/0.67R123) are tested and compared [37]. The system behaviors at two different operation strategies are addressed [38].

2. Experimental setup of ORC system

A 3 kW ORC experimental prototype is adopted, as shown in **Figure 1**. It includes three loops: heating loop, ORC loop and cooling loop. The photo of experimental layout and the main facilities of ORC system are plotted in **Figure 2**.

2.1 Heating loop

An electric heater using conduction oil is used as the simulated heat source, within four electrical heating rods having the capacity of 80 kW. An axial pump adjusted the mass flow rates of conductive oil, ensuring the heat source temperatures ranging from 110 to 140°C. Meanwhile, the evaporator heat transfer rate can be changed by adjusting the input power of electric heater, which is controlled by the four electrical heating rods.

2.2 ORC loop

The ORC loop is made up of four major components: a plunger pump, an evaporator, a scroll-type expander and a condenser. It should be noted that R123 is used in this study because of its better thermal efficiency and environmental performance. The pump supplies the working fluid to the evaporator where the working fluid is heated and vaporized by the conductive oil. The high pressure vapor flows into the expander and its enthalpy is converted into work. The low pressure vapor exits the expander and is led to the condenser where it is liquefied by water. The liquid is available at the condenser outlet, and then it is pumped back to the evaporator and a new cycle begins.

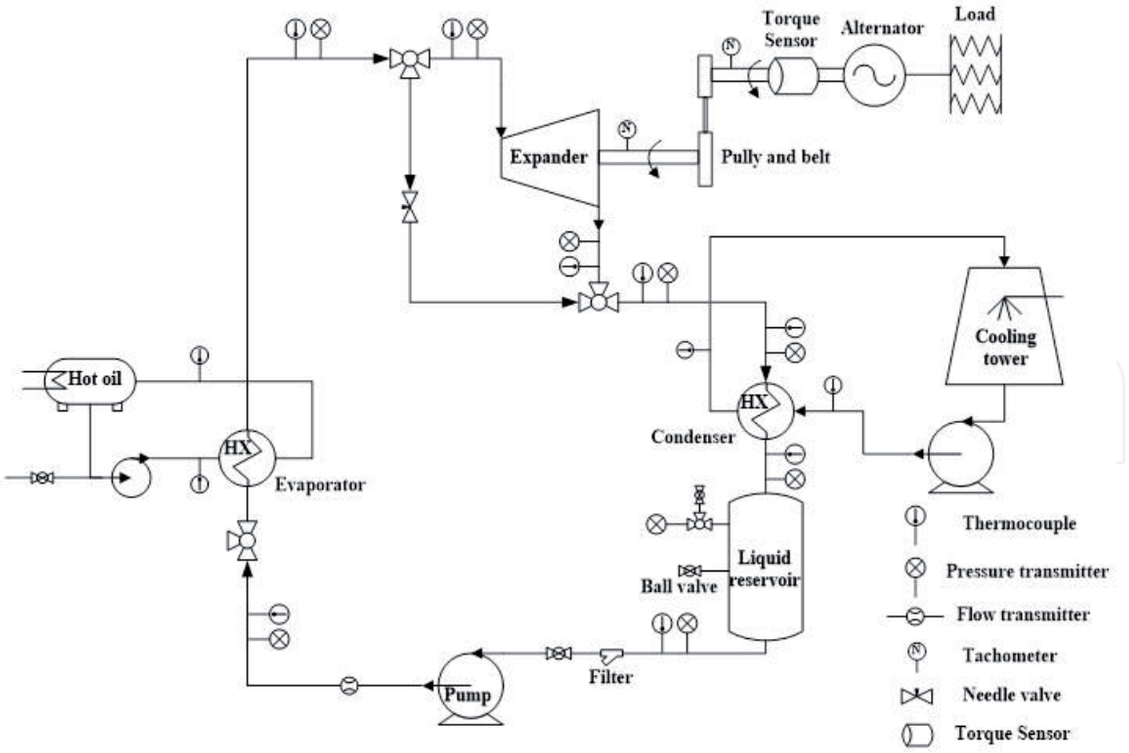

Figure 1.
Schematic diagram of an ORC system.

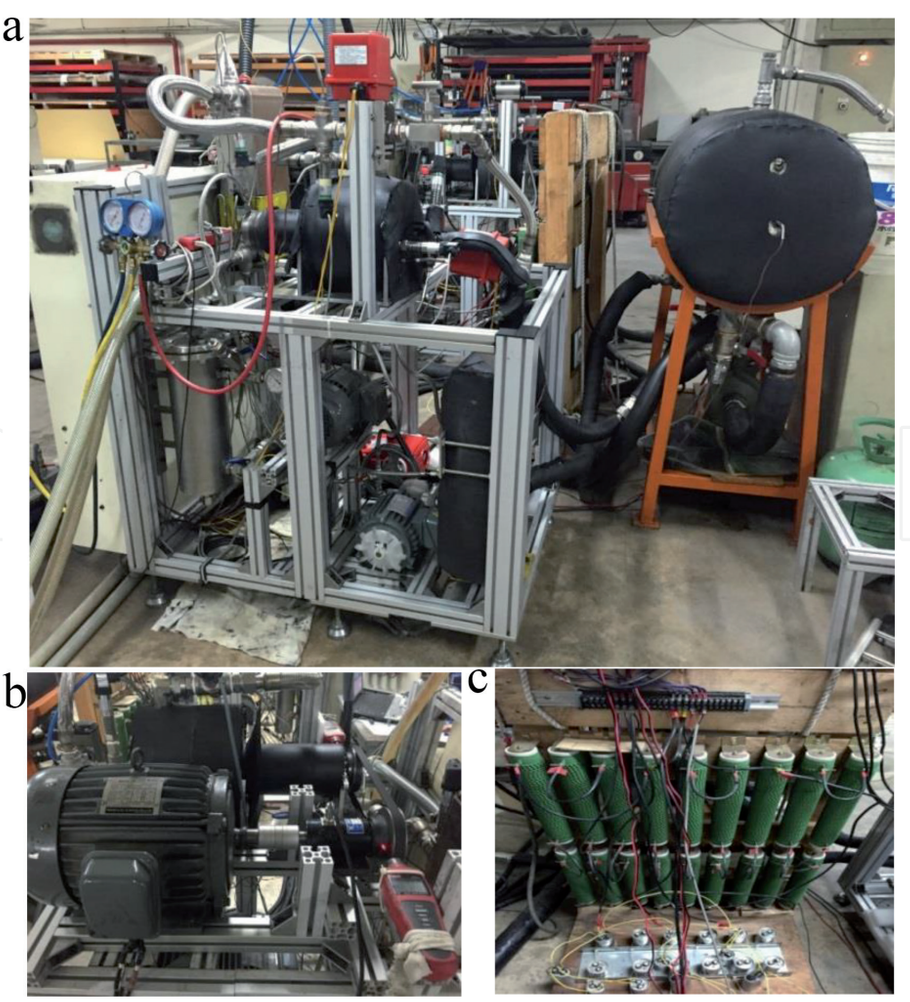

Figure 2.
The photos of (a) experimental setup, (b) the expander generator set, and (c) the electrical load.

The plunger pump is controlled by a frequency converter, with the achievable maximum delivered pressure head and flow rate are 50 bars and 18 L/min, respectively. The pump power consumption can be obtained by measuring the voltage and current, while the pump shaft power can be calculated by the thermodynamic parameters at the inlet and outlet of pump.

The evaporator and condenser are plate heat exchangers with the same heat transfer area of 4.157 m^2. Asbestos board and insulating foam are equipped around the evaporator and condenser to avoid the heat loss.

A scroll-type expander, which was modified from commercial oil-free scroll type air compressor with a built-in volume ratio of three, is employed. The expander shaft power is transferred to the three-phase permanent-magnet generator by pulley and belt. The alternating current produced by permanent-magnet generator is converted to direct current using three bridge rectifier. The frequency of direct current is adjusted by the electrical resistance and capacitance to meet the grid frequency requirements.

2.3 Cooling loop

The cooling tower is installed at roof and extras the heat from condenser to air environment. Therefore, the cooling inlet water is fluctuated by the environmental temperature. The needle value is used to adjust the mass flow rate of cooling water.

3. Thermodynamic analysis method

It should be noted that the thermodynamic properties of pure and mixture working fluids are obtained based on NIST Refprop [39]. Based on the measured temperatures and pressures, the corresponding enthalpies and entropies for every state can be obtained. **Figure 3** shows *T-s* plot of the thermodynamic cycle. For the expander, the vapor working fluid (state 1) enters the expander to generate power output, and then exits (state 2). The evaporator heat transfer rate (Q_{eva}), which is heated by the conductive oil, is

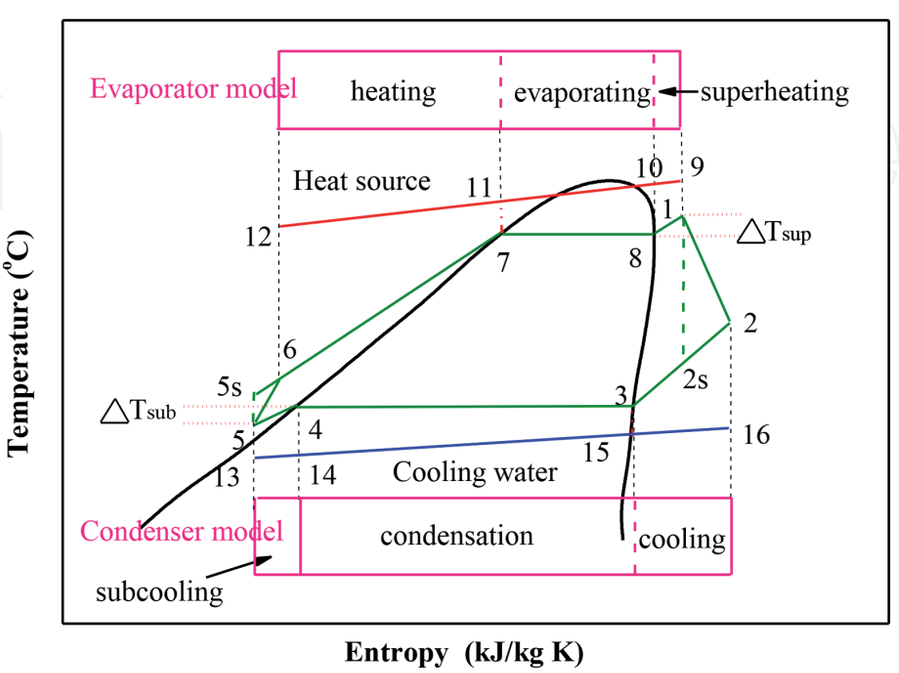

Figure 3.
T-s plot of the ORC cycle, as well as the evaporator and condenser model.

$$Q_{eva} = m(h_1 - h_6) \tag{1}$$

The expander power output is calculated according to the thermodynamic state at expander inlet and outlet, while the expander shaft power is measured by torque meter, which can be obtained by torque and rotating speed. Meanwhile, the ideal isentropic expansion process in expander is from 1 to 2 s, while the real one is from 1 to 2. The expander power output ($W_{p,exp}$) and shaft power ($W_{sh,exp}$) can be expressed as follows:

$$W_{p,exp} = m(h_1 - h_2) \tag{2}$$

$$W_{sh,exp} = \frac{2\pi}{60} M_{exp} n_{exp} \tag{3}$$

where h_1 and h_2 are the inlet and outlet enthalpy of expander, which is determined by the measured pressure and temperature; M_{exp} is the torque, and n_{exp} is the rotating speed, which is measured by tachometer.

The electrical power produced by generator can be calculated by measuring the current and voltage. The pump shaft power can be calculated by the measured pressure and temperature, while the power consumption is measured by pump frequency converter. To better understand the portion of the electricity output for driving the pump, back work ratio (BWR) is proposed to represent the ratio between pump consumption and electricity output, which can be expressed as:

$$\mathrm{BWR} = \frac{W_{ele,pump}}{W_{ele,exp}} \tag{4}$$

The thermal efficiency and system generating efficiency can be expressed as:

$$\eta_{th,cal} = \frac{(h_1 - h_2) - (h_6 - h_5)}{h_1 - h_6} \tag{5}$$

$$\eta_{th,test} = \frac{W_{sh} - W_p}{Q_{eva}} \tag{6}$$

$$\eta_{ele} = \frac{W_{ele,exp} - W_{ele,p}}{Q_{eva}} \tag{7}$$

4. Effects of different operation parameters

The operation parameters have a significant influence on system performance. Based on the 3 kW ORC experimental prototype, the steady-state operation test is discussed at first, and then the four operation parameters on system behavior are examined.

4.1 Steady-state operation test

The heat input is used to control the heat source temperature, while the working fluid pump frequency is adopted to adjust the working fluid mass flow rate. The experimental data is collected at every 5 s. The test is recorded when the heat source temperatures are within a small fluctuation below ±0.5°C. One point is the average value of a 20 min steady operation. When the mass flow rate is in range

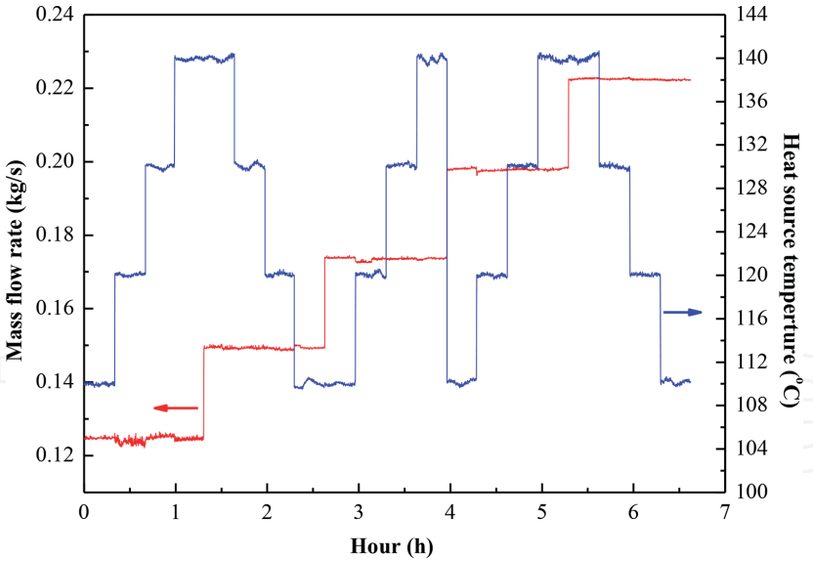

Figure 4.
Variation of heat source temperatures and mass flow rates with time.

of 0.124–0.222 kg/s and heat source temperature is in range of 110–140°C, the variation of heat source temperatures and mass flow rates with time are plotted in **Figure 4**. Obviously, the mass flow rate and heat source temperature have a relatively stable variation.

Taking the mass flow rate of 0.124 kg/s and heat source temperature of 110°C as an example, the detailed steady-state operation characteristic for 20 min steady operation is shown in **Figure 5**. It can be seen that the pump outlet pressure (**Figure 5b**), expander inlet pressure (**Figure 5c**), and mass flow rate of working fluids (**Figure 5f**) have a relatively strong variation, indicating that a control strategy for the pump and expander is necessary.

4.2 Effect of mass flow rate

The working fluid mass flow rate is adjusted by the pump frequencies. **Figure 6** plots the variation of thermal efficiency with mass flow rate at different heat source temperatures. It can be seen that the thermal efficiencies for different heat source temperatures have a similar behavior of a decreasing trend with mass flow rate, which may be attributed to the increasing heat input. Meanwhile, the thermal efficiency keeps rising with the heat source temperature, which may be attributed to the increasing power output. It also can be found that when the mass flow rate is 0.124 kg/s and the heat source temperature is 140°C, the thermal efficiency owns a maximum value of 5.14%.

Figure 7 shows the variation of system generating efficiency with mass flow rate at different heat source temperatures. As the mass flow rate increases, the system generating efficiency keeps decreasing for a heat source temperature smaller than 120°C, whereas represents a parabolic trend for a heat source temperature higher than 130°C. Meanwhile, the system generating efficiency keeps rising with the heat source temperature. A highest system generating efficiency of 3.25% is appeared for a mass flow rate of 0.198 kg/s and a heat source temperature of 140°C. The system generating efficiency is in range of 0.94–3.25%.

4.3 Effect of pressure drop

The pressure drop denotes the expander inlet pressure minus the pump inlet pressure. The variation of electrical power, thermal efficiency and system generating

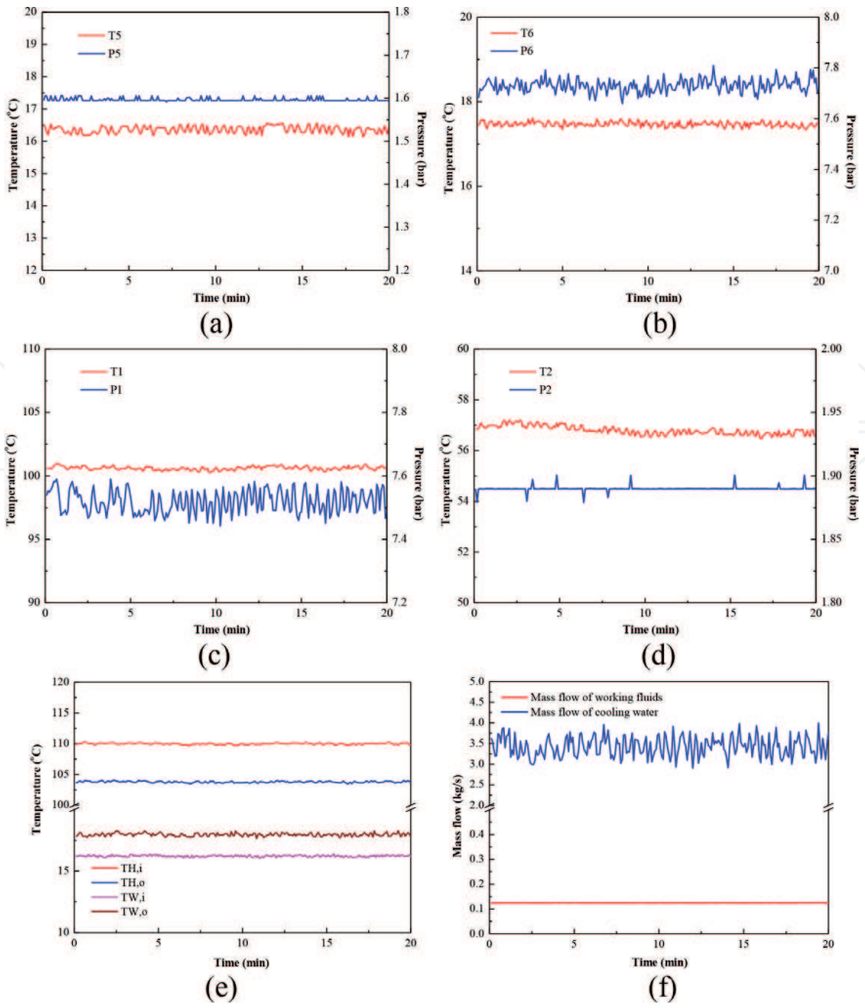

Figure 5.
Variation of system parameters with time. (a) pump inlet pressure and temperature, (b) pump outlet pressure and temperature, (c) expander inlet pressure and temperature, (d) expander outlet pressure and temperature, (e) cooling water inlet and outlet temperature and heat source inlet and outlet temperature, (f) mass flow rates of working fluid and cooling water.

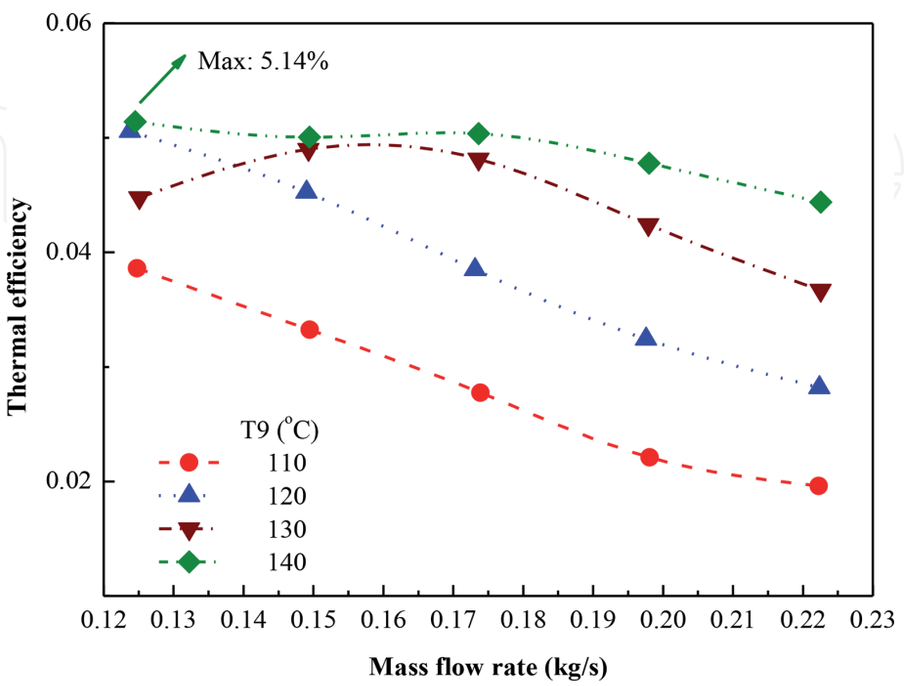

Figure 6.
Variation of thermal efficiency with mass flow rate at different heat source temperatures.

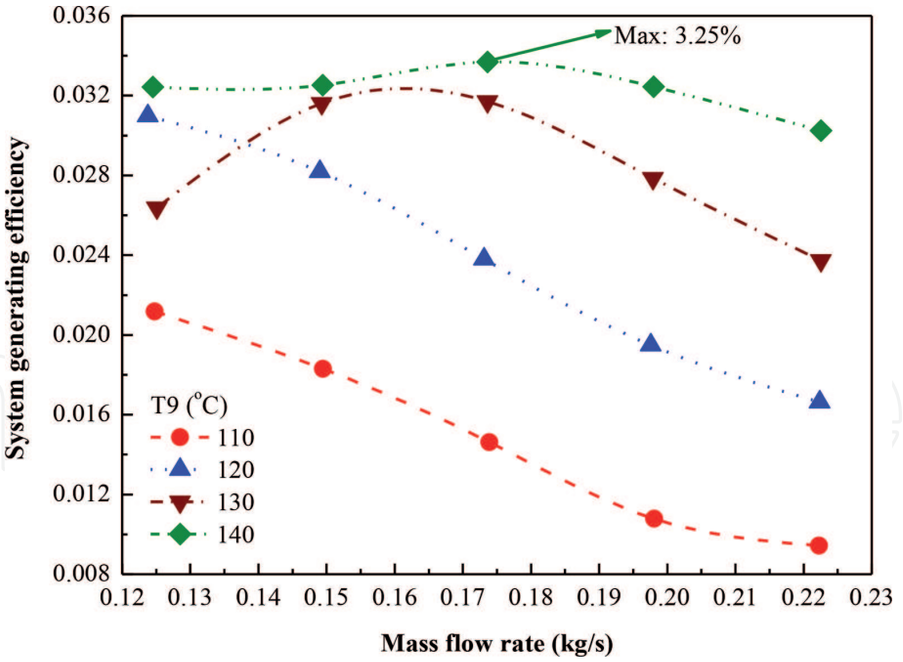

Figure 7.
Variation of system generating efficiency with mass flow rate at different heat source temperature.

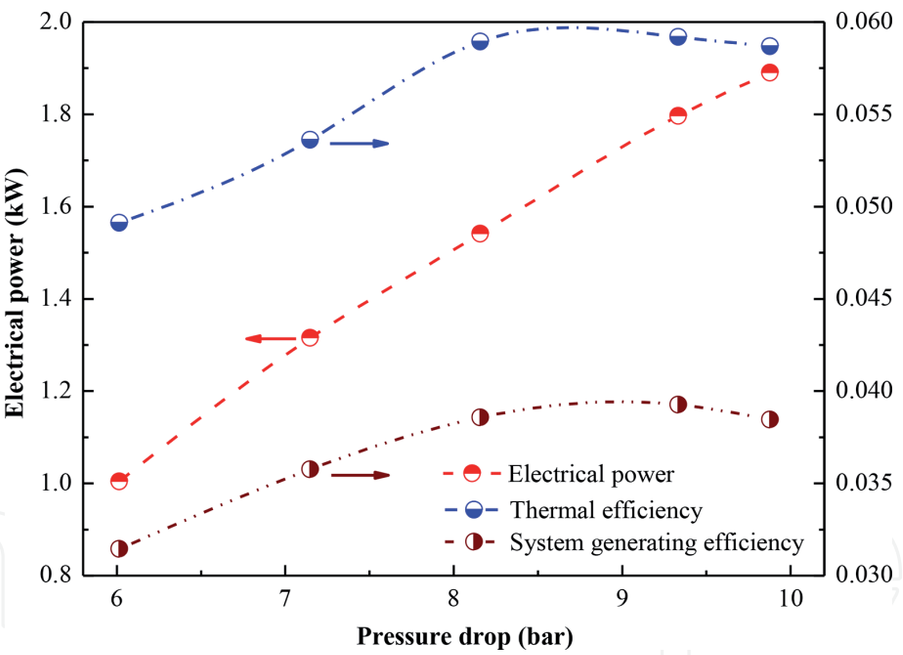

Figure 8.
Variation of electrical power, thermal efficiency and system generating efficiency with pressure drop.

efficiency are demonstrated in **Figure 8**. As the pressure drop increases, the system generating efficiency and thermal efficiency own a similar behavior of an increase first and then a slightly decrease, whereas the electrical power goes up. The increasing heat input causes the parabolic trend for thermal efficiency and system generating efficiency. A higher pressure drop denotes a higher investment cost of heat exchanger for pressure-bearing requirement. And therefore, the optimum pressure drop is 8.16 bar, with the corresponding thermal efficiency of 5.89% and system generating efficiency of 3.86%. It also can be found that the maximum thermal efficiency of 5.92% and maximum system generating efficiency of 3.93% are obtained with the corresponding pressure drop of 9.33 bar.

4.4 Effect of degree of superheating

The variation of electrical power, thermal efficiency and system generating efficiency with degree of superheating are displayed in **Figure 9**. It can be seen that the electrical power, thermal efficiency and system generating efficiency yield a small variation with the degree of superheating, which is in line with the theoretical study. The main reason is that the degree of superheating has a negligible effect on the power output. The electrical power of 1.35 kW, thermal efficiency of 6.48% and system generating efficiency of 3.91% can be owned.

4.5 Effect of condenser temperature

The needle value is used to adjust the cooling water mass flow rate, while the working fluid mass flow rate is set to be 0.10 kg/s. The variation of electrical power, thermal efficiency and system generating efficiency with condenser temperature are

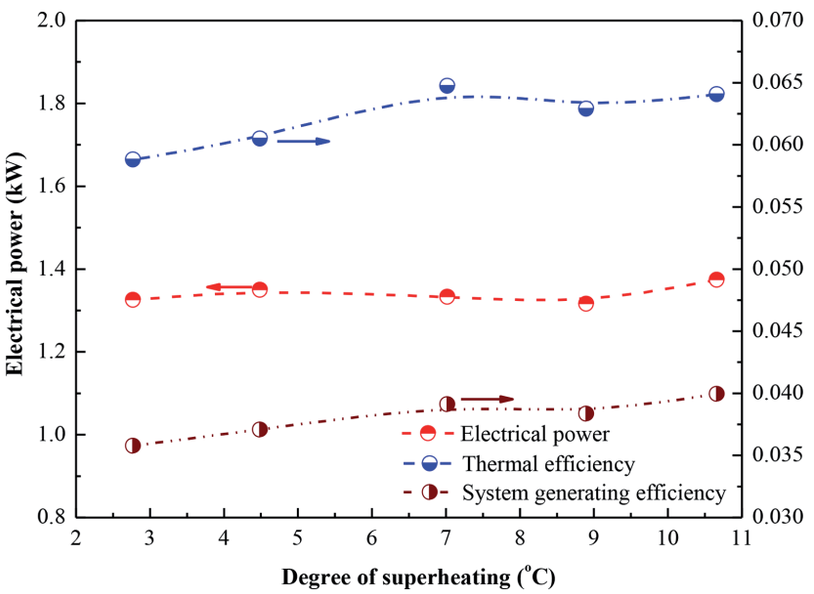

Figure 9.
Variation of electrical power, thermal efficiency and system generating efficiency with degree of superheating.

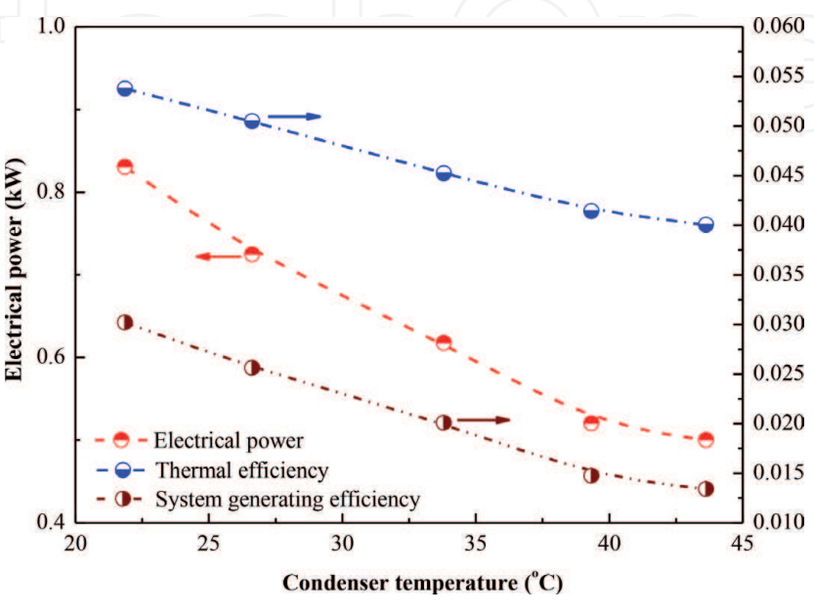

Figure 10.
Variation of electrical power, thermal efficiency and system generating efficiency with condenser temperature.

demonstrated in **Figure 10**. As the condenser temperature increases, the electrical power, thermal efficiency and system generating efficiency own a similar behavior of a decrease trend. The main reason is that the rising condenser temperature decreases the expander enthalpy difference, resulting in the decrease in the power output. When the condenser temperature increases from 22 to 43°C, the electrical power decreases from 0.83 to 0.50 kW, while the thermal efficiency decreases from 3.02 to 1.34%.

Based on the parametric analysis, the pressure drop has a relatively effect on the system performance, indicating that improving the system overall performance should give priority to increase the pressure drop. Meanwhile, the optimum electrical power and thermal efficiency are 1.89 kW and 5.92%, respectively. The maximum thermal efficiency does not represent the highest electrical power, which is in line with the theoretical study.

5. Operation characteristics comparison between mixture and pure working fluids

To better compare the operation characteristics between the pure working fluids and mixture working fluids, two pure working fluids (R245fa, R123) and two mixtures working fluids (0.67R245fa/0.33R123 and 0.33R245fa/0.67R123) are tested.

BWR denotes the ratio between pump consumption and electricity output. For theoretical study, the pump consumption is always ignore, whereas it accounts for a large proportion for ORC experimental prototype. The BWR for R245fa, R123 and their mixtures are displayed in **Figure 11**. As the mass flow rate increases, the BWR for different working fluids own a parabolic trend. There is an optimum mass flow rate to the lowest BWR. Meanwhile, the mixture working fluids yield a relatively higher BWR than the pure working fluids. 0.67R245fa/0.33R123 owns the highest BWR, while R123 yields the lowest BWR. BWR is in range of 11.86–23.22%, indicating that improving the pump operation characteristics is one way to enhance the ORC performance.

Figure 12 shows the expander shaft power with mass flow rate for R245fa, R123 and their mixtures. It can be seen that as the mass flow rate increases, the expander shaft power for R245fa, 0.67R245fa/0.33R123 and 0.33R245fa/0.67R123 present a

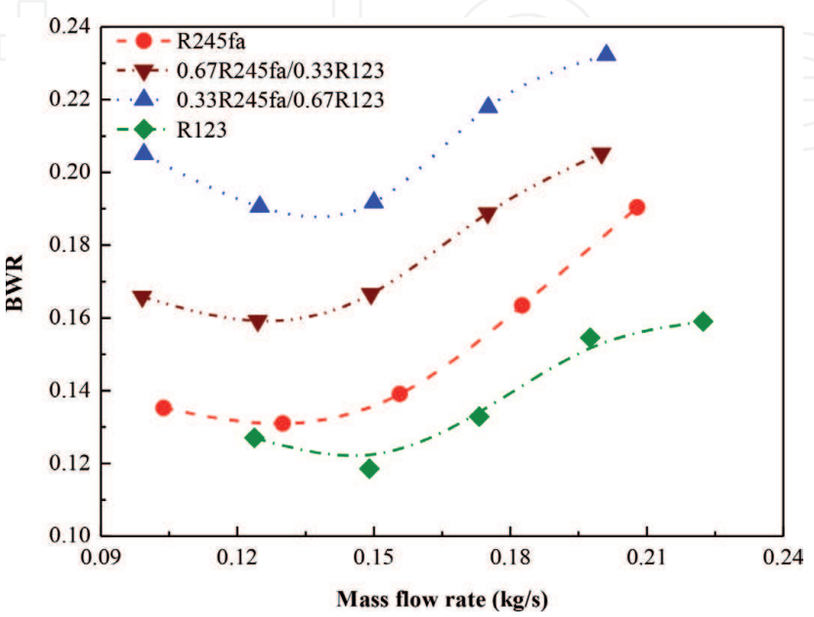

Figure 11.
Variation of BWR with mass flow rate for R245fa, R123 and their mixtures.

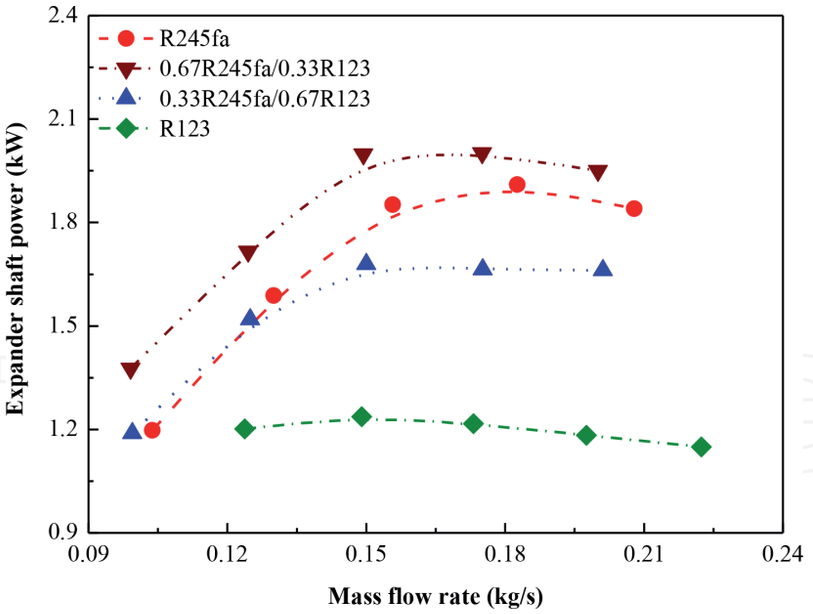

Figure 12.
Variation of expander shaft power with mass flow rate for R245fa, R123 and their mixtures.

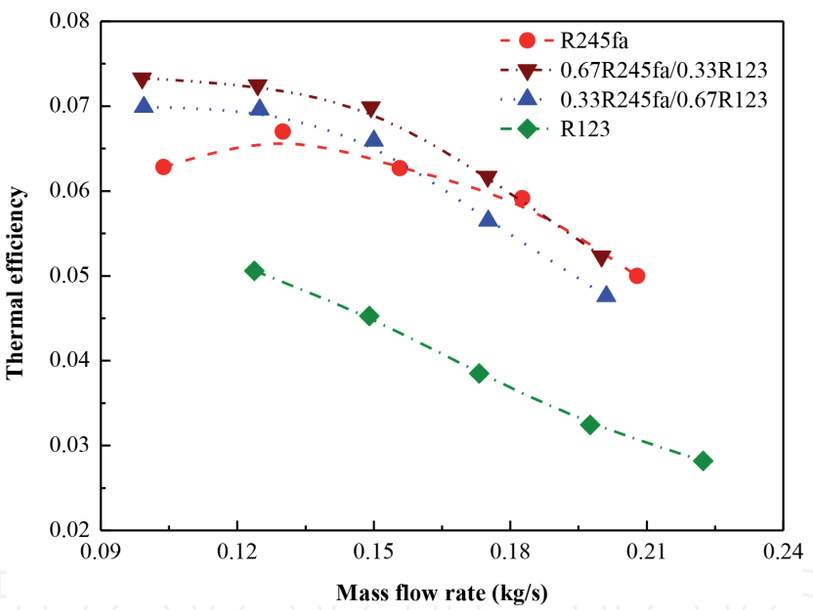

Figure 13.
Variation of thermal efficiency with mass flow rate for R245fa, R123 and their mixtures.

similar trend of increase first and then decrease, while that of R123 almost has no change. The highest expander shaft power is obtained by 0.67R245fa/0.33R123, while the lowest one is got by R123. One optimum mass flow rate is existed to ensure the highest expander shaft power. The maximum expander shaft power for R245fa of 2.76 kW, 0.67R245fa/0.33R123 of 2.85 kW, 0.33R245fa/0.67R12 of 2.46 kW and R123 of 1.82 kW are obtained.

The thermal efficiencies for R245fa, R123 and their mixtures are plotted in **Figure 13**. As observed, as the mass flow rate increases, the thermal efficiencies for 0.33R245fa/0.67R123, 0.67R245fa/0.33R123 and R123 keep decreasing, whereas that of R245 presents a parabolic trend. The thermal efficiency is determined by the net power output and heat input. The main reason is the comprehensive effect of the increasing net power output and heat input. It also can be found that the mixture working fluids have a relatively higher thermal efficiency than the

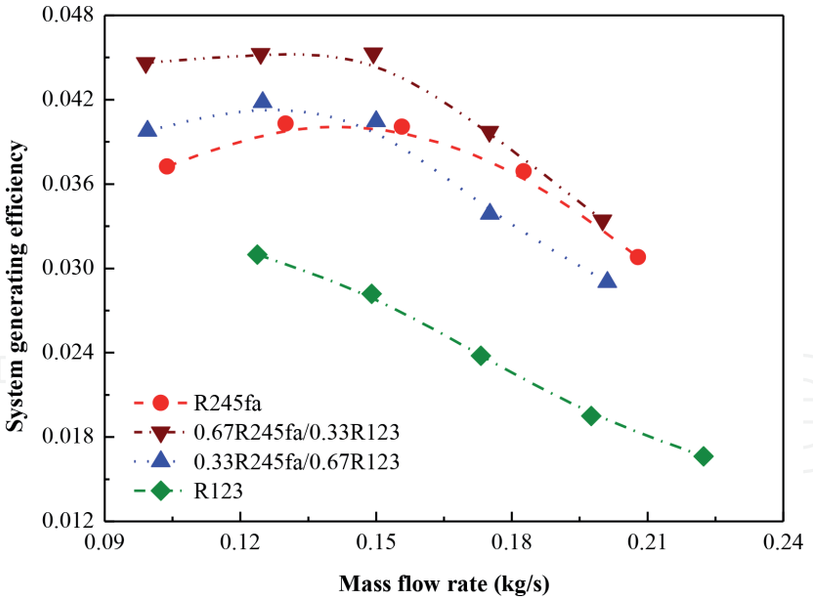

Figure 14.
Variation of system generating efficiency with mass flow rate for R245fa, R123 and their mixtures.

pure working fluids. The maximum thermal efficiencies for R245fa of 6.70%, 0.67R245fa/0.33R123 of 7.33%, 0.33R245fa/0.67R123 of 6.99% and R123 of 5.06% are obtained. 0.67R245fa/0.33R123 owns the highest maximum thermal efficiency of 7.33, 9.4% higher than that of R245fa and 44.86% higher than that of R123.

Figure 14 shows the system generating efficiencies with mass flow rate for R245fa, R123 and their mixtures. The system generating efficiencies for different working fluids have a same trend with the thermal efficiency (as shown in **Figure 13**). The comprehensive influence of heat input and net electricity output enables the parabolic trend in system generating efficiency. The maximum system generating efficiencies for R245fa of 4.03%, 0.67R245fa/0.33R123 of 4.53%, 0.33R245fa/0.67R123 of 4.18% and R123 of 3.10% are yielded. Meanwhile, the corresponding mass flow rate for maximum system generating efficiencies of R245fa, 0.67R245fa/0.33R123, 0.33R245fa/0.67R123 and R123 are 0.130, 0.149, 0.125 and 0.124 kg/s, respectively. 0.67R245fa/0.33R123 owns the highest system generating efficiency of 4.53%, which is 12.41% higher than that of R245fa.

Through the experimental comparison between the pure and mixture working fluids, it indicates that whether the mixtures exhibit better thermodynamic performance than the pure working fluids depend on the operation parameters and mass fraction of mixtures. Meanwhile, the mixture working fluids obtain a higher expander shaft power but a relatively higher BWR, indicating enhancement in pump is necessary for ORC application.

6. System behaviors at different operation strategies

To ensure that ORC can operate at different zone, two operation strategies are proposed: stand alone and gird connect operation strategies. The mass flow rates and expander rotating speed with heat input for standalone and gird connect operation strategies are displayed in **Figure 15**. As the heat input increases, the mass flow rate for standalone operation strategy is in range of 0.153–0.359 kg/s, while that of grid connect operation strategy increases from 0.230 to 0.420 kg/s. Meanwhile, the expander rotating speed for standalone operation strategy keeps rising from 2320 to 2983 rpm, whereas that of grid connect operation strategy keeps constant of 3600 rpm.

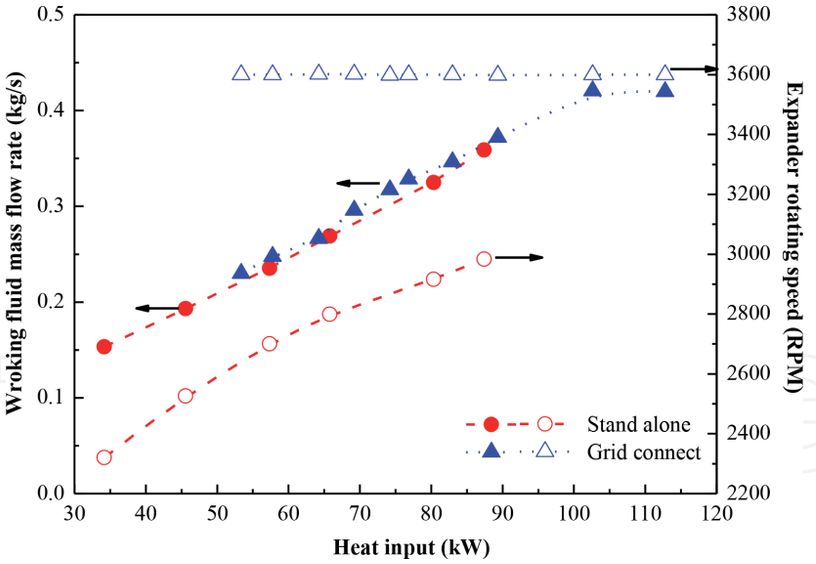

Figure 15.
Variation of working fluid mass flow rates and expander rotating speed with heat input for standalone and gird connect operation strategies.

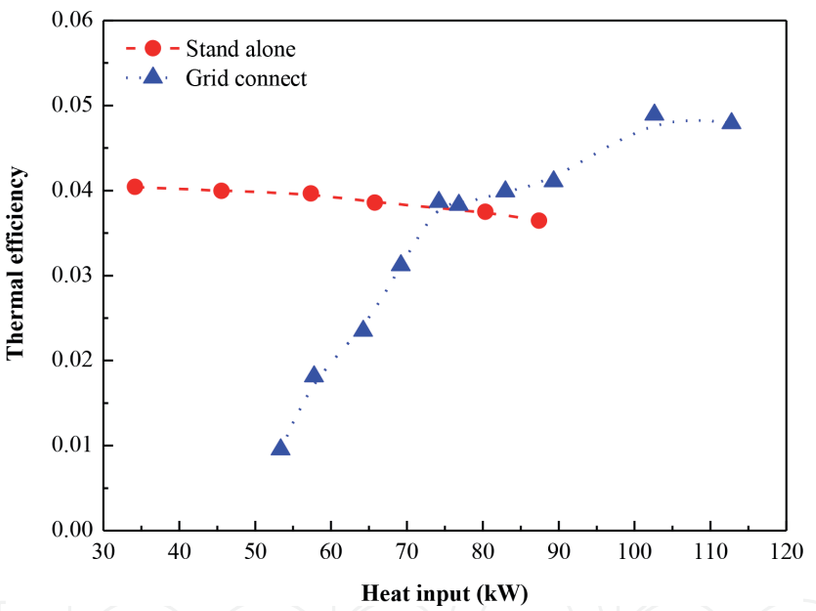

Figure 16.
Variation of thermal efficiencies with heat input for standalone and gird connect operation strategies.

Figure 16 shows the thermal efficiencies with heat input for standalone and gird connect operation strategies. When the heat input increases from 34.18 to 87.40 kW, the thermal efficiency for standalone operation strategy decreases 4.04–3.64%, which may be attributed to the comprehensive effect of increasing heat input. However, for the gird connect operation strategy, the thermal efficiency increases from 0.96–4.89% with heat input. Meanwhile, when the heat input is lower than 74.20 kW, the stand alone operation strategy owns a relatively higher thermal efficiency than the gird connect operation strategy, but an opposite trend for the heat input higher than 74.20 kW. When the heat input is 102.62 kW, the gird connect operation strategy yields the highest thermal efficiency of 4.89%.The system generating efficiencies with heat input for standalone and gird connect operation strategies are demonstrated in **Figure 17**. The system generating efficiencies for standalone and gird connect operation strategies present a similar trend with the thermal efficiencies (as shown in **Figure 16**). The maximum system generating

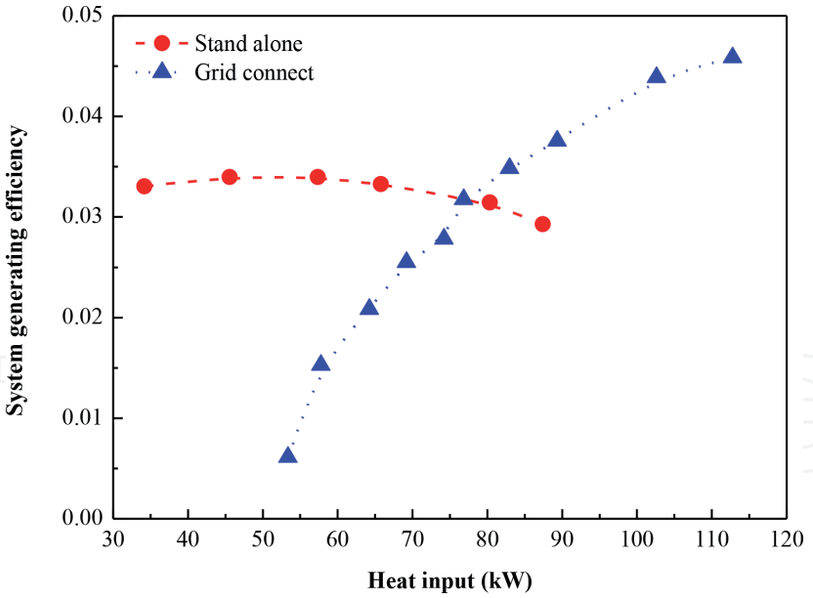

Figure 17.
Variation of system generating efficiencies with heat input for standalone and gird connect operation strategies.

efficiency for gird connect operation strategy is 4.59%, which is 35% higher than that of standalone operation strategy approaching of 3.40%.

7. Conclusion

Power conversion systems based on organic Rankine cycles have been identified as a potential technology especially in converting low-grade waste heat into electricity. This chapter presents the detailed operation characteristic of a small-scale ORC. The effect of mass flow rate, pressure drop, degree of superheating and condenser temperature on thermal efficiency and system generating efficiency are examined. Two pure working fluids (R245fa, R123) and two mixtures working fluids (0.67R245fa/0.33R123 and 0.33R245fa/0.67R123) are tested and compared. The system behaviors at two different operation strategies are addressed. The pressure drop has a relatively effect on the system performance, indicating that improving the system overall performance should give priority to increase the pressure drop. The maximum thermal efficiency does not represent the highest electrical power, which is in line with the theoretical study. The degree of superheating exhibits insensitive on the electrical power. There is an optimum mass flow rate to ensure the minimum BWR. Whether the mixtures exhibit better thermodynamic performance than the pure working fluids depend on the operation parameters and mass fraction of mixtures. Meanwhile, the mixture working fluids obtain a higher expander shaft power but a relatively higher BWR. The expander rotating speed for standalone operation strategy keeps rising from 2320 to 2983 rpm, whereas that of grid connect operation strategy keeps constant of 3600 rpm. When the heat input is lower than 74.20 kW, the stand alone operation strategy owns a relatively higher thermal efficiency than the gird connect operation strategy, but an opposite trend for the heat input higher than 74.20 kW.

Acknowledgements

This research work has been supported by the Ministry of Science and Technology, Taiwan under the grants of Contract No. MOST 107-2221-E-027-091, and by "Research Center of Energy Conservation for New Generation of Residential,

Commercial, and Industrial Sector" from The Featured Areas Research Center Program within the framework of the Higher Education Sprout Project by the Ministry of Education (MOE) in Taiwan. The authors are grateful for National Natural Science Foundation of China (51806081), the Natural Science Foundation of Jiangsu Province (BK20180882), the China Postdoctoral Science Foundation (2018 M632241) and the Open Foundation Program of Key Laboratory of Efficient Utilization of Low and Medium Grade Energy (Tianjin University), the Ministry of Education of China (201806-402).

Conflict of interest

The author declared that there is no conflict of interest.

Author details

Tzu-Chen Hung[1*] and Yong-qiang Feng[2]

1 Department of Mechanical Engineering, National Taipei University of Technology, Taipei, Taiwan

2 School of Energy and Power Engineering, Jiangsu University, Zhenjiang, China

*Address all correspondence to: tchung@ntut.edu.tw

References

[1] Feng YQ, Hung TC, Zhang Y, Li BX, Yang JF, Shi Y. Performance comparison of low-grade organic Rankine cycles (ORCs) using R245fa, pentane and their mixtures based on the thermoeconomic multi-objective optimization and decision makings. Energy. 2015;**99**:2018-2029. DOI: 10.1016/j.energy.2015.10.065

[2] Feng YQ, Zhang YN, Li BX, Yang JF, Shi Y. Comparison between regenerative organic Rankine cycle (RORC) and basic organic Rankine cycle (BORC) based on thermoeconomic multi-objective optimization considering exergy efficiency and levelized energy cost (LEC). Energy Conversion and Management. 2015;**96**:58-71. DOI: 10.1016/j.enconman.2015.02.045

[3] Feng YQ, Hung TC, Greg K, Zhang YN, Li BX, Yang JF. Thermoeconomic comparison between pure and mixture working fluids for low-grade organic Rankine cycles (ORCs). Energy Conversion and Management. 2015;**106**:859-872. DOI: 10.1016/j.enconman.2015.09.042

[4] Tian H, Shu GQ, Wei HQ, Liang XY, Liu LN. Fluids and parameters optimization for the organic Rankine cycles (ORCs) used in exhaust heat recovery of internal combustion engine (ICE). Energy. 2012;**47**:125-136. DOI: 10.1016/j.energy.2012.09.021

[5] Tchanche B, Papadakis G, Lambrinos G, Frangoudakis A. Fluid selection for a low-temperature solar organic Rankine cycle. Applied Thermal Engineering. 2009;**29**:2468-2476. DOI: 10.1016/j.applthermaleng.2008.12.025

[6] Dong BS, Xu GQ, Luo X, Zhuang LH, Quan YK. Potential of low temperature organic Rankine cycle with zeotropic mixtures as working fluid. Energy Procedia. 2017;**105**:1489-1494. DOI: 10.1016/j.egypro.2017.03.444

[7] Chang JC, Hung TC, He YL, Zhang WP. Experimental study on low-temperature organic Rankine cycle utilizing scroll type expander. Applied Energy. 2015;**155**:150-159. DOI: 10.1016/j.apenergy.2015.05.118

[8] Muhammad U, Imran M, Lee DH, Park BS. Design and experimental investigation of a 1 kW organic Rankine cycle system using R245fa as working fluid for low-grade waste heat recovery from steam. Energy Conversion and Management. 2015;**103**:1089-1100. DOI: 10.1016/j.enconman.2015.07.045

[9] Mathias JA, Johnston JR, Cao JM, Priedeman DK, Christensen RN. Experimental testing of gerotor and scroll expanders used in, and energetic and exergetic modeling of, an organic Rankine cycle. Journal of Energy Resources Technology Transactions ASME. 2009;**131**:21-24. DOI: 10.1115/1.3066345

[10] Carraro G, Pallis P, Leontaritis AD, Karellas S, Vourliotis P, Rech S, et al. Experimental performance evaluation of a multi-diaphragm pump of a micro-ORC system. Energy Procedia. 2017;**129**:1018-1025. DOI: 10.1016/j.egypro.2017.09.232

[11] Yang XF, Xu JL, Miao Z, Zou JH, Yu C. Operation of an organic Rankine cycle dependent on pumping flow rates and expander torques. Energy. 2015;**90**:1-15. DOI: 10.1016/j.energy.2015.07.121

[12] Xu W, Zhang JY, Zhao L, Deng S, Zhang Y. Novel experimental research on the compression process in organic Rankine cycle (ORC). Energy Conversion and Management. 2017;**137**:1-11. DOI: 10.1016/j.enconman.2017.01.025

[13] Lei B, Wang JF, Wu YT, Ma CF, Wang W, Zhang L, et al. Experimental

study and theoretical analysis of a Roto-Jet pump in small scale organic Rankine cycles. Energy Conversion and Management. 2016;**111**:198-204. DOI: 10.1016/j.enconman.2015.12.062

[14] Zeleny Z, Vodicka V, Novotny V, Mascuch J. Gear pump for low power output ORC—An efficiency analysis. Energy Procedia. 2017;**129**:1002-1009. DOI: 10.1016/j.egypro.2017.09.227

[15] Bianchi G, Fatigati F, Murgia S, Cipollone R, Contaldi G. Modeling and experimental activities on a small-scale sliding vane pump for ORC-based waste heat recovery applications. Energy Procedia. 2016;**101**:1240-1247. DOI: 10.1016/j.egypro.2016.11.139

[16] Wu TM, Liu JH, Zhang L, Xu XJ. Experimental study on multi-stage gas-liquid booster pump for working fluid pressurization. Applied Thermal Engineering. 2017;**126**:9-16. DOI: 10.1016/j.applthermaleng.2017.07.159

[17] Yang YX, Zhang HG, Xu YH, Yang FB, Wu YT, Lei B. Matching and operating characteristics of working fluid pumps with organic Rankine cycle system. Applied Thermal Engineering. 2018;**142**:622-631. DOI: 10.1016/j.applthermaleng.2018.07.039

[18] Landelle A, Tauveron N, Revellin R, Haberschill P, Colasson S, Roussel V. Performance investigation of reciprocating pump running with organic fluid for organic Rankine cycle. Applied Thermal Engineering. 2017;**113**:962-969. DOI: 10.1016/j.applthermaleng.2016.11.096

[19] Meng FX, Zhang HG, Yang FB, Hou XC, Lei B, Zhang L. Study of efficiency of a multistage centrifugal pump used in engine waste heat recovery application. Applied Thermal Engineering. 2017;**110**:779-786. DOI: 10.1016/j.applthermaleng.2016.08.226

[20] Bianchi M, Branchini L, Casari N, De PA, Melino F, Ottaviano S, et al. Experimental analysis of a micro-ORC driven by piston expander for lowgrade heat recovery. Applied Thermal Engineering. 2019;**148**:1278-1291. DOI: 10.1016/j.applthermaleng.2018.12.019

[21] Yang YX, Zhang HG, Xu YH, Zhao R, Hou XC, Liu Y. Experimental study and performance analysis of a hydraulic diaphragm metering pump used in organic Rankine cycle system. Applied Thermal Engineering. 2018;**132**:605-612. DOI: 10.1016/j.applthermaleng.2018.01.001

[22] Bianchi G, Fatigati F, Murgia S, Cipollone R. Design and analysis of a sliding vane pump for waste heat to power conversion systems using organic fluids. Applied Thermal Engineering. 2017;**124**:1038-1048. DOI: 10.1016/j.applthermaleng.2017.06.083

[23] Sun HC, Qin J, Hung TC, Hua HY, Ya PG, Lin CH. Effect of flow losses in heat exchangers on the performance of organic Rankine cycle. Energy. 2019;**172**:391-400. DOI: 10.1016/j.energy.2019.01.131

[24] Xi H, Zhang HH, He YL, Huang ZH. Sensitivity analysis of operation parameters on the system performance of organic Rankine cycle system using orthogonal experiment. Energy. 2019;**172**:435-442. DOI: 10.1016/j.energy.2019.01.072

[25] Borsukiewicz-Gozdur A. Pumping work in the organic Rankine cycle. Applied Thermal Engineering. 2013;**51**:781-786. DOI: 10.1016/j.applthermaleng.2012.10.033

[26] Dong BS, Xu GQ, Cai Y, Li HW. Analysis of zeotropic mixtures used in high-temperature organic Rankine cycle. Energy Conversion and Management. 2014;**84**:253-260. DOI: 10.1016/j.enconman.2014.04.026

[27] Garg P, Kumar P, Srinivasan K, Dutta P. Evaluation of isopentane, R-245fa and their mixtures as working fluids for organic Rankine cycles. Applied Thermal Engineering. 2013;**51**(1):292-300. DOI: 10.1016/j.applthermaleng.2012.08.056

[28] Lecompte S, Ameel B, Ziviani D, van den Broek M, De Paepe M. Exergy analysis of zeotropic mixtures as working fluids in organic Rankine cycles. Energy Conversion and Management. 2014;**85**:727-739. DOI: 10.1016/j.enconman.2014.02.028

[29] Zhao L, Bao JJ. The influence of composition shift on organic Rankine cycle (ORC) with zeotropic mixtures. Energy Conversion and Management. 2014;**83**:203-211. DOI: 10.1016/j.enconman.2014.03.072

[30] Liu Q, Duan Y, Yang Z. Effect of condensation temperature glide on the performance of organic Rankine cycles with zeotropic mixture working fluids. Applied Energy. 2014;**115**:394-404. DOI: 10.1016/j.apenergy.2013.11.036

[31] Pu W, Yue C, Han D, He W, Liu X, Zhang Q, et al. Experimental study on organic Rankine cycle for low grade thermal energy recovery. Applied Thermal Engineering. 2016;**94**:221-227. DOI: 10.1016/j.applthermaleng.2015.09.120

[32] Molés F, Navarro-Esbrí J, Peris B, Mota-Babiloni A. Experimental evaluation of HCFO-1233zd-E as HFC-245fa replacement in an organic Rankine cycle system for low temperature heat sources. Applied Thermal Engineering. 2016;**98**:954-961. DOI: 10.1016/j.applthermaleng.2016.01.011

[33] Jung HC, Taylor L, Krumdieck S. An experimental and modelling study of a 1 kW organic Rankine cycle unit with mixture working fluid. Energy. 2015;**81**:601-614. DOI: 10.1016/j.energy.2015.01.003

[34] Li T, Zhu J, Fu W, Hu K. Experimental comparison of R245fa and R245fa/R601a for organic Rankine cycle using scroll expander. International Journal of Energy Research. 2015;**39**(2):202-214. DOI: 10.1002/er.3228

[35] Feng YQ, Hung TC, Wu SL, Lin CH, Li BX, Huang KC, et al. Operation characteristic of a R123-based organic Rankine cycle depending on working fluid mass flow rates and heat source temperature. Energy Conversion and Management. 2017;**131**:55-68. DOI: 10.1016/j.enconman.2016.11.004

[36] Yang SC, Hung TC, Feng YQ, Wu CJ, Wong KW, Huang KC. Experimental investigation on a 3 kW organic Rankine cycle for low grade waste heat under different operation parameters. Applied Thermal Engineering. 2017;**113**:756-764. DOI: 10.1016/j.applthermaleng.2016.11.032

[37] Feng YQ, Hung TC, He YL, Wang Q, Wang S, Li BX, et al. Operation characteristic and performance comparison of organic Rankine cycle (ORC) for low-grade waste heat using R245fa, R123 and their mixtures. Energy Conversion and Management. 2017;**144**:153-163. DOI: 10.1016/j.enconman.2017.04.048

[38] Feng YQ, Hung TC, Su TY, Wang S, Wang Q, Yang SC, et al. Experimental investigation of a R245fa-based organic Rankine cycle adapting two operation strategies: Stand alone and grid connect. Energy. 2017;**141**:1239-1253. DOI: 10.1016/j.energy.2017.09.119

[39] NIST Standard Reference Database 23. NIST thermodynamic and transport properties of refrigerants and refrigerant mixtures REFROP, Version 9.0. 2010